

Accelerating Parallel I/O Via Hardware-Algorithm Co-Designed Adaptive Lossy Compression

Chengming Zhang, Sian Jin, Jiannan Tian, Dingwen Tao
Washington State University
Pullman, WA, USA
{chengming.zhang,sian.jin,jiannan.tian,dingwen.tao}@wsu.edu

Tong Geng, Ang Li
Pacific Northwest National Laboratory
Richland, WA, USA
{tong.geng,ang.li}@pnnl.gov

Abstract

As parallel computers continue to grow to exascale, the amount of data that needs to be saved or transmitted is exploding. To this end, many previous works have studied using error-bounded lossy compressors to reduce the data size and improve the I/O performance. However, little work has been done for effectively offloading lossy compression onto FPGA-based SmartNICs to reduce the compression overhead. In this paper, we propose a hardware-algorithm co-design for an efficient and adaptive lossy compressor for scientific data on FPGAs (called CEAZ), which is the first lossy compressor that can achieve high compression ratios and throughputs simultaneously. Specifically, we propose an efficient Huffman coding approach that can adaptively update Huffman codewords online based on codewords generated offline, from a variety of representative scientific datasets. Moreover, we derive a theoretical analysis to support a precise control of compression ratio under an error-bounded compression mode, enabling accurate offline Huffman codewords generation. This also helps us create a fixed-ratio compression mode for consistent throughput. In addition, we develop an efficient compression pipeline by adopting cuSZ’s dual-quantization algorithm to our hardware use cases. Finally, we evaluate CEAZ on five real-world datasets with both a single FPGA board and 128 nodes (to accelerate parallel I/O). Experiments show that CEAZ outperforms the second-best FPGA-based lossy compressor by $2\times$ of throughput and $9.6\times$ of ratio. It also improves MPI_File_write and MPI_Gather throughputs by up to $28.1\times$ and $36.9\times$, respectively.

1 Introduction

Today’s large-scale parallel applications can generate large volumes of scientific data for post-hoc analysis and visualization. However, since the development of storage and networking hardware is much slower than that of computing power and memory capacity [5], the I/O and network bandwidth are becoming the main bottlenecks for HPC applications to achieve high performance on a large scale. I/O and communication costs can quickly overwhelm the overall performance as parallel computers grow towards exascale. For instance, a well-known cosmological simulation code Nyx [1] can generate up to 2.8 TB of data for a single snapshot under a simulation resolution of 4096^3 , requiring to save a total of 2.8 PB data, when running the simulation for 5 times with 200 snapshots dumped per run.

Such a large amount of data is often generated in a parallel manner from a scaling number of ranks, on which each

holds a proportion of the data and must introduce an extra collective communication to dump the entire snapshot to the file system. This process takes an unprecedented challenge to I/O bandwidths and storage systems on today’s parallel computers [5, 26, 48, 49]. Therefore, it is urgent to develop effective data reduction methods to reduce the size of data movement between memories and storage systems.

One of the most effective ways to address this challenge is using data compression. The data partition in each rank is compressed before sending it to the storage system via an interconnected network. This can reduce both I/O overhead and storage consumption. However, traditional lossless compression can only provide a limited compression ratio to the scientific dataset by usually up to $2\times$ [37]. Thus, error-bounded lossy compressors such as SZ [8, 26, 41] and ZFP [27] have been developed to provide a much higher compression ratio while only introducing controllable distortion of data. Many prior studies have demonstrated the effectiveness of using those error-bounded lossy compressors for scientific data reduction [5, 8, 16, 21, 22, 26, 27, 30, 31, 41, 42] and improving I/O performance. [14, 34, 50].

While error-bounded lossy compressors on CPUs can provide a high compression ratio, their low throughputs unavoidably cause relatively high performance overheads to applications, which often offset the performance benefit from saving and loading compressed data of less sizes. Thus, we need to develop a high-throughput lossy compressor to effectively accelerate parallel I/O for HPC applications. Recently, both SZ and ZFP teams started to develop and release their GPU and FPGA implementations. On one hand, GPU’s massive SIMT parallelism enables high throughput. However, during the lossless compression step of SZ algorithm, Huffman encoding and decoding [19] results in a random memory access pattern [44]. This causes serious divergence issues, inevitably leading to low GPU memory bandwidth utilization and performance. On the other hand, FPGAs offer many advantages, such as configurability, high energy efficiency, low latency, and low price [13], and have been a viable and popular option at scales for smart network interface cards (SmartNICs) [11, 35], which are being increasingly used in data centers to offload networking functions from host processors [18]. Thus, this makes FPGA-based SmartNICs ideal platforms to offload compression and accelerate I/O.

The state-of-the-art FPGA-based lossy compressor is only capable of about 8 GB/s throughput [39], which is still much lower than the throughput of PCIe3/4 and InfiniBand. This precludes their use in real application scenarios. There are

several challenges to implement a high-throughput lossy compression on FPGAs with a relatively high compression ratio: (1) Most of lossy compression algorithms involve multiple stages which have strong data dependency. (2) It is infeasible to simply add more compression pipelines on FPGAs with limited resources. Thus, we need to deeply optimize the algorithm to effectively utilize the hardware resources.

To address these challenges, in this work, we focus on designing an efficient lossy compression algorithm that is suitable for FPGA hardware, and offload it onto FPGA-based SmartNICs to accelerate parallel I/O. Specifically, we propose a hardware-algorithm co-designed efficient and adaptive lossy compressor (zip) (CEAZ), which is the first lossy compressor to achieve high compression ratio and throughput simultaneously. CEAZ adopts a dual quantization strategy [44] to completely remove data dependency and instantiates multiple pipelines to process input data in parallel. Unlike cuSZ that implements dual-quantization using massive GPU threads, we implement the dual quantization in CEAZ using a pipelined manner, which is more suitable for FPGA architecture. Moreover, different from existing FPGA-based lossy compressors such as GhostSZ [51] and waveSZ [43] that statically build trees in Huffman coding for every data chunk, CEAZ dynamically determines whether to update codewords by building a new tree or use previous/offline codewords according to the distribution of current symbol frequencies, leading to a high throughput. Thus, CEAZ can efficiently and effectively reduce the data size and significantly increase the parallel I/O performance. Our contributions are summarized as follows:

- We propose an efficient Huffman coding approach that adaptively updates Huffman codewords online based on our offline Huffman codewords, which are generated from a variety of representative scientific datasets. It can reduce the data dependency in Huffman coding and dramatically improve the compression throughput.
- We derive a theoretical analysis to support a precise control of compression ratio under the error-bounded compression mode, which can align quantization-code histograms of different datasets and enable an accurate generation of offline Huffman codewords. It also helps us develop a fixed-ratio compression mode, which is important to guarantee a consistent throughput in data transfer. Our work is the first prediction-based lossy compressor to enable fixed-rate compression.
- We develop an efficient compression pipeline by adapting the dual-quantization algorithm to our hardware use case.
- We evaluate CEAZ with five real-world scientific datasets in both serial and parallel processing. Experiments show that CEAZ outperforms the state-of-the-art solution by 2× in throughput and 9.6× in ratio on a single FPGA board. Moreover, CEAZ can improve the MPI_File_write and MPI_Gather throughputs by up to 28.1× and 36.9×, respectively, with 128 nodes from Summit supercomputer.

The rest of this paper is organized as follows. In Section 2, we discuss the background and challenges. In Section 3, we present the design of CEAZ. In Section 4, we evaluate CEAZ on six scientific datasets and present our results. In Section 5, we summarize our work and discuss future work.

2 Background and Motivation

2.1 Floating-Point Data Compression

Floating-point data compression has been studied for decades. The data compressors can be split into two categories: lossless compression and lossy compression. In comparison to lossy compression, lossless compression such as FPZIP [28] and FPC [4] can only provide limited compression ratios (typically up to 2:1 for most scientific data) due to the significant randomness of the ending mantissa bits, especially for large scientific floating-point data [37].

Lossy compression, on the other hand, can compress data with little information loss in the reconstructed data. Compared to lossless compression, lossy compression can provide a much higher compression ratio while still maintaining useful information for scientific discoveries. Many lossy compressors supporting floating-point data were proposed and designed for visualization. Thus, many lossy compressors employ techniques directly inherited from lossy compression of images, such as variations of wavelet transforms, coefficient prioritization, and vector quantization. While such compressors may be adequate for visualization, they do not provide error controls on demand for scientific studies.

In recent years, a new generation of lossy compressors for scientific floating-point data has been proposed and developed, such as SZ [8, 26, 41, 44] and ZFP [7, 27]. Both lossy compressors can provide multiple compression modes, such as error-bounded mode and fixed-rate mode to introduce error control or compression ratio control. Error-bounded mode requires users to set an error bound, and fixed-rate mode means that users can set a target bitrate. Compared to ZFP which utilizes Discrete Fourier transform to manipulate data information, SZ predicts each data point’s value by its neighboring data points in a multidimensional space with an adaptive predictor (mainly using a Lorenzo predictor [20]). Next, it performs an error-controlled linear-scaling quantization to convert all floating-point values to an array of integer numbers. Lastly, it performs a customized Huffman coding and lossless compression to shrink the data size significantly. This helps SZ provide a unified error distribution between original and reconstructed data within the user-set error-bound range, which fully utilizes the error tolerance space and provides a high compression ratio [8, 26, 30, 40, 41].

SZ was first developed for CPU architectures, and has released the CUDA implementation (called cuSZ) [44]. Compared to lossy compression on CPUs, GPU-based lossy compression can provide much higher (de)compression throughputs [21]. CuSZ [44] and cuZFP [7] are existing GPU-based

implementations of SZ and ZFP, respectively, which are capable of achieving tens to hundreds of GB/s (de)compression throughputs. However, these approaches are not very efficient on FPGAs, which have much lower clock frequencies compared to GPUs. Moreover, the FPGA chip space limitations prevent fitting too many instances of compression pipelines on chip. But, FPGA implementations offer several advantages over GPU implementations: (1) FPGAs can inherently provide low latency as well as deterministic latency for real-time applications. (2) FPGAs provide a high degree of user customization, and their implementations are easier to be integrated into other systems.

2.2 FPGA-based Lossy Compression

Existing works have shown that significant performance speedups can be achieved by offloading lossy compression onto hardware. GhostSZ [51] is the first implementation of SZ-1.0 [9] lossy compression on FPGAs. GhostSZ improves throughput by 10~85× over the SZ with a similar compression ratio and peak signal-to-noise ratio (PSNR). However, SZ-1.0 is a deprecated version which suffers from low prediction accuracy which results in low compression ratios [43].

waveSZ [43] is another hardware implementation of SZ lossy compression. It adopts a wavefront memory layout to fit into SZ algorithm to alleviate the data dependency during the prediction process. It improves the compression ratio and throughput over GhostSZ. However, waveSZ has several drawbacks: (1) It just alleviates the data dependency using wavefront memory but does not eliminate it. As a result, its throughput does not exceed 1 GB/s. (2) Its wavefront memory layout involves rearranging data before compression, and this overhead would be relatively high when processing a large amount of data. (3) It only focuses on accelerating the prediction stage without handling the high overhead of Huffman coding. This, however, is the main bottleneck after fully removing the data dependency in prediction.

BurstZ [39] is a variant of the 1-dimensional ZFP algorithm and also implemented onto FPGAs. BurstZ can provide a high throughput (8 GB/s), but it suffers from a significantly lower compression ratio drop compared with the original ZFP algorithm. For example, the original ZFP algorithm achieves 21× compression ratio on the NWChem dataset [33] with an error bound of 0.001, whereas BurstZ only achieves 4.7× compression using the same error bound. Besides, the 8GB throughput is much smaller than the throughput of current PCIe3/4 and InfiniBand. In addition, ZHW [52] is an FPGA-based lossy compressor based on the ZFP algorithm, but it is not error-bounded. So, we take BurstZ as the current state-of-the-art FPGA implementation of ZFP.

2.3 MPI Collectives and MPI-I/O

Message Passing Interface (MPI) [15] contains two main types of operations related to parallel I/O, i.e., MPI-IO operations and collective operations. On the one hand, MPI-IO is a

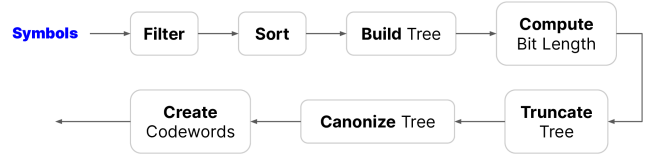


Figure 1. The process of canonical Huffman encoding.

fundamental HPC middleware for parallel I/O. Many parallel I/O systems such as parallel HDF5 [12] and ADIOS [29] are built based on it. In MPI-IO, data is moved between files and processes by issuing read and write calls. The data access routines can be individual or collective. By using a collective routine, processes are coordinated with each other to optimize access to I/O devices. On the other hand, MPI collective operations such as scatter, gather and reduce play an important role in many HPC applications for communication. Considering that many applications use dedicated I/O nodes to periodically collect/distribute data from compute nodes and then write/read to the file system asynchronously, we also use MPI_Gather/Scatter in this paper to evaluate our compressor in this use scenario.

2.4 Research Challenges

High Overhead of Huffman Coding. Given a set of symbols, Huffman coding generates codewords based on the evidence that not all symbols have the same probability. Instead of using fixed-length codewords, Huffman coding uses variable-length codewords based on the relative frequency of different symbols. The principle is to use fewer bits to represent frequent symbols and more bits to represent infrequent symbols. Even though variable-length codewords can provide high compression ratio in our scenario, Huffman coding has high overhead in terms of latency, area, and power [25]. To achieve a high overall compression throughput, certain key challenges in Huffman coding need be addressed.

Challenge of Codewords Generation. The first challenge is to build a Huffman tree and generate codewords within limited hardware clock cycles to meet high-throughput requirements. Our goal is to accelerate MPI collective I/O in real time through compression. So we hope to reduce the compression latency as much as possible. In addition, generating codewords needs 7 steps: filter, sort, create tree, compute bit length, truncate tree, canonize tree and create codewords, as illustrated in Figure 1. This procedure is a serial process that is hard to be parallelized by FPGAs or GPUs. We make full use of the characteristics of the FPGAs to speed up this process by pipelining. However, the latency presented in Figure 4 is still relatively large.

Challenge of Predefined Codewords. Inspired by [25], we will use predefined codewords at the beginning and update the codewords during the runtime. This method introduces the second challenge: how to generate suitable codewords to cover the features of all the scientific datasets?

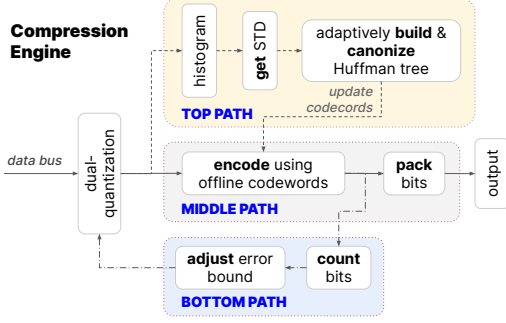


Figure 2. Design of our proposed lossy compression engine CEAZ.

3 Design Methodology

3.1 Overview of CEAZ Engine

We show our proposed lossy compression engine in Figure 2. It has three main dataflow paths. On the top dataflow path, we preprocess float-point data using a dual quantization algorithm [44] (abbreviated as dual-quant), which generates integers as symbols for the following Huffman coding. We collect frequencies of symbols using a histogram and calculate the standard deviation (STD) of frequencies. According to the STD value, we will decide whether to build a new Huffman tree based on the symbol frequencies or not (will be discussed in the next section).

Figure 3 shows our dual-quant pipeline design. Dual-quant is a novel two-phase prediction-quantization approach, which can completely eliminate the data dependency in the prediction and quantization steps. Our dual-quant consists of two steps: prequantization and postquantization. Given a float point data d , we first quantize it based on the user-set error bound and convert it to an integer data d' . After the prequantization, we can calculate its predicted value based on its neighboring values (denoted $\text{neighboring}(d')$) using Lorenzo predictor (denoted ℓ), $p = \ell(\text{neighboring}(d'))$. The second step, called postquantization, computes the difference δ between the predicted value and the prequantized value. δ will be compressed by Huffman compression. Since the dual-quant part has no data dependency, we could instantiate N pipelines to process N float-point data in parallel. On the middle dataflow path, we directly encode symbols using existing codewords for seeking high throughput. The encoder can find the codeword corresponding to each symbol and output it. We then pack variable-length encoded (compressed) symbols to save the storage space. On the bottom

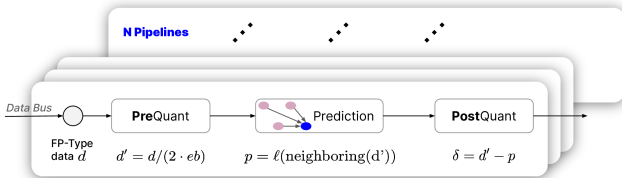


Figure 3. Design of our adopted dual-quantization pipeline.

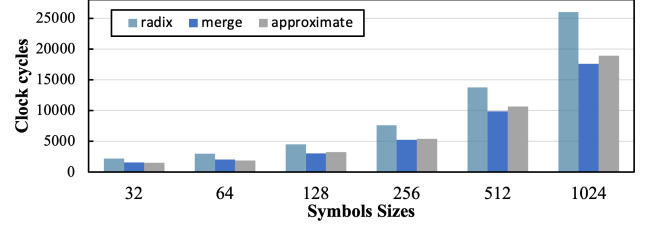


Figure 4. Our Huffman encoder latency with different symbol sizes. dataflow path, we feed back total bits of encoded symbols to estimate compression ratio, and then adjust the error bound.

Our proposed compression engine has two working modes: fixed accuracy (i.e., error bounded) and fixed ratio (i.e., fixed bit-rate). The fixed-accuracy mode ensures information loss of compressed data is within the specific error bound, whereas the fixed-ratio mode ensures the transfer of compressed data has a consistent throughput. For the fixed-accuracy mode, we need to define an upper bound of errors that can be tolerated by applications and keep using this error bound through the whole compression process. For the fixed-ratio mode, we can set a suitable error bound to achieve a target compression ratio, as a higher error bound leads to a higher compression ratio. Specifically, we adjust the error bound as follows: (1) We estimate the compression ratio by $C = \frac{\text{TotalBits(original data)}}{\text{TotalBits(compressed data)}}$, where $\text{TotalBits(original data)} = W * N$. Here W is the bit-rate of original data; for single/double floating-point data, W is 32/64 bits per value; N is the total number of data points that have been compressed. (2) We calculate the compressed and target bit-rates by $B = \frac{W}{C}$ and $B_{\text{target}} = \frac{W}{C_{\text{target}}}$, respectively. (3) We adjust the error bound by Equation (2) (will be discussed in Section 3.2.2).

3.2 Efficient and Adaptive Huffman Coder

3.2.1 Fast approximate sort. In order to build the Huffman tree, we must sort the symbols based on their frequencies after we filter out symbols with a frequency of zero. Previous works [23, 46] use radix sort to reduce the utilization of hardware resources. However, we find that radix sort typically takes more than 30% of the total time when we break down the execution time of generating codewords. This is because the time complexity of radix sort is $O(d \times (n + b))$ (where b is the base to represent numbers and d is the maximum number of digits) with $d = 32$ and $b = 10$ typically.

We note that the frequencies of symbols that are generated by Lorenzo predictor and linear-scaling quantization [41] are symmetric, as shown in prior studies [22]. We verify this in our experiments with 1024 symbols, as shown in Figure 5 (symmetric with respect to symbol 513). This feature inspires us to use an approximate sort to improve the efficiency, since Huffman coding can accept the approximately sorted symbols, which would not notably degrade the compression ratio. Specifically, assuming A is an unsorted array with symbols, and O stores sorted symbols. We initialize two indexes l and h to represent the quantization codes to the left and right of

Algorithm 1: Proposed fast sort based on Lorenzo predictor's feature.

Result: A approximately sorted array

```

1  S: defined structure contains two members: symbol, and its frequency
2  A: input array, its data type is S, len: length of input array, i: index of A
3  p: index of symbol 513 in A, m: index of the midpoint of A, l: index, h: index
4  O: output sorted array, j: index of O
5  t: loop count
6  l = p - 1, h = p + 1, j = len - 2, O[len - 1] = A[p]
7  if p ≤ m then
8    |   t = p
9  else
10   |   t = len - p - 1
11 end
12 for i ← 1, t do
13   if A[l].frequency ≤ A[h].frequency then
14     |   O[j] = A[h]
15     |   O[j - 1] = A[l]
16   else
17     |   O[j] = A[l]
18     |   O[j - 1] = A[h]
19   end
20   l = l - 1, h = h + 1, j = j - 2
21 end
22 CopyRemaining(A, O) /* copy remaining data from A to O */

```

the middle quantization code. We compare the frequencies of the two quantization codes and store them in a correct order into *O*. We then decrease *l* by 1 and increase *h* by 1 and repeat this process till all quantization codes are sorted.

We describe our proposed approximate sort algorithm in Algorithm 1 in detail. It has the time complexity of $O(\frac{n}{2})$, which is lower than the time complexity of radix sort and merge sort. We compare the total time of Huffman coding with different sort algorithms using 1024 symbols. The results shown in Figure 4 illustrate that our approximate sort saves the total Huffman coding time by up to 27% over the second-best radix sort. More details about our experimental platform will be presented in Section 4.

3.2.2 Offline Huffman codewords generation. On the premise of meeting the acceptable reduction in compression ratio, we propose to combine offline and online Huffman codewords generation strategies in order to improve the throughput as much as possible. As shown in figure 2, the symbols generated at the beginning by dual-quant will be encoded by offline codewords directly; at the same time, we also collect the frequencies of symbols. We will generate new Huffman codewords if the change of STD of symbol frequencies is greater than the threshold τ . τ is a hyper-parameter, and we will discuss it in the next section.

We generate offline codewords based on the following three steps: (1) We set a suitable error bound to let our compressor have a similar compression ratio on different datasets. (2) We collect symbol frequencies on different datasets. (3) We calculate the average symbol frequencies from collected frequencies. The average symbol frequencies are used to generate offline codewords. In order to make offline codewords representative and promising for high compression ratio, we collect symbol frequencies based on all the real-world

datasets from the Scientific Data Reduction Benchmarks (SDRBench) [36]. Figure 8 shows the ratio degradation by using the offline codewords (will be showed in Section 4.3).

Using different error bounds to compress the same dataset results in different histograms of quantization codes (i.e., different distributions of symbol frequencies). For example, using a larger error bound results in a tighter histogram of quantization codes compared to using a smaller error bound. In extreme cases where very large error bounds are used, there can be only a few quantization codes for Huffman coding. To make the offline codewords adaptive for a wide range of datasets, we must choose suitable error bounds for multiple scientific datasets, which can result in a similar histogram of quantization codes after employing the Lorenzo predictor. In other words, we must control the error bound for each dataset to provide a similar ratio. Instead of using a trial-and-error approach to search the suitable error bound for every dataset, we provide a theoretical analysis to predict the error bound given a target ratio based on one-time sampling.

A naive solution to align different datasets with a similar compression ratio is to use the same value-ranged-based relative error bound¹ instead of the same absolute error bound. While using the same value-ranged-based relative error bound for different datasets can reduce the divergence of their quantization-code histogram, it cannot guarantee that the compression ratio of different datasets is similar to each other. In our experiment, we identify the compression ratio range of 4~13× when using the same value-ranged-based relative error bound for multiple scientific datasets. Our proposed solution considers the efficiency of Huffman coding affected by error bound to accurately estimate the error bound for a target compression ratio. We assume the bit-rate of quantization code after Huffman encoding is:

$$\text{mean}(L) = \sum_{i=0}^n P(s_i) L(s_i) \approx \sum_{i=0}^n P(s_i) \log_2 P(s_i), \quad (1)$$

where n is the number of different Huffman code, P is the probability of given code s_i , L is the length of given code s_i . We further represent the Huffman code length based on its probability with binary base-2 numeral system. Note that in our case, 1024 symbols are used for Huffman coding and thus are sufficient for this simplification. Consider a given error bound eb can provide a bit-rate of B , when doubling the error bound to $2eb$, the quantization-code histogram also shrinks accordingly where the total number of symbols is reduced by 2× and the possibility of each symbol is increased by 2×. In this case, the bit-rate should be:

$$\begin{aligned} B' &= \sum_{i=0}^{n/2} P'(s_i) \log_2 P'(s_i) \approx \sum_{i=0}^{n/2} (P(s_{2i-1}) \log_2 P'(s_{2i-1}) \\ &\quad + P(s_{2i}) \log_2 P'(s_{2i})) - 1 = B - 1 \end{aligned} \quad (2)$$

¹Note that unlike the pointwise relative error that is compared with each data value, value-range-based relative error is compared with value range.

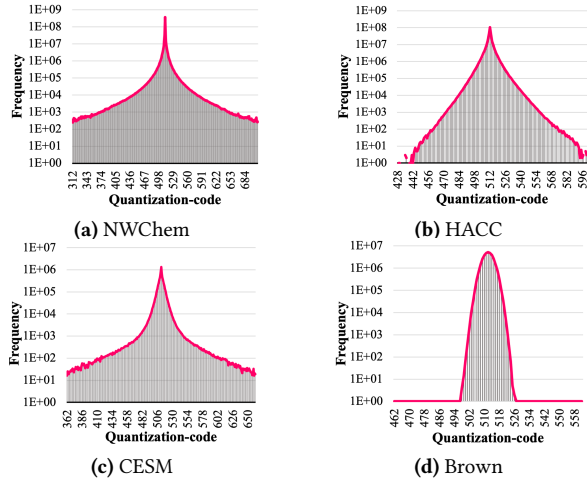


Figure 5. Distribution of symbol frequencies on four scientific datasets, i.e., NWChem [33], HACC [17], CESM [6], and Brown [3].

Thus, we conclude that by doubling the error bound, the bit-rate should increase by 1. Furthermore, we can derive that if the compression bit-rate is B under the error bound eb , then under the new error bound Neb the predicted bit-rate is $B' = B - \log_2 N$. Note that the SZ algorithm uses previous data points' quantized values to predict the value of current point based on Lorenzo prediction, which means different error bounds would affect the shape of quantization-code histogram. However, based on our experiments, this only applies to very large error bounds and hence few quantization bins. In our case, we simplify this to a fixed quantization-code histogram shape under different error bounds, yielding a precise $2\times$ shrink when doubling the error bound.

With the above analysis, we can simply compress each scientific dataset once with the same value-ranged-based relative error bound eb and compute the optimized error bound eb' for the target bit-rate B_{target} based on the current bit-rate B by $eb' = 2^{B-B_{\text{target}}} eb$.

3.2.3 Adaptive online codewords updates. In general, on one hand, the more frequently we update the codewords, the closer we can get to the optimal codewords in terms of compression ratio. On the other hand, too frequently updating codewords may decrease the compression ratio, since the newly generated codewords need to be stored. Moreover, if we do not update the codewords, the compression ratio may decrease as well, because the old codewords are too outdated to reflect current distribution of symbol frequencies. In order to solve this problem, we use two effective metrics to determine when to generate new codewords: (1) the storage overhead of codewords and (2) the change of distribution of symbol frequencies.

For example, suppose we have S symbols and S codewords. Each codeword is B bits on average after canonization process. We have $\text{size}(\text{codewords}) = S \times B$. Our target compression ratio is C . The bit-rate of original data is W . For single or double floating-point data set, the bit width is 32

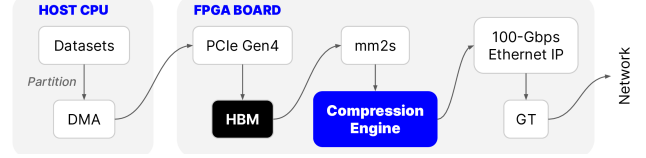


Figure 6. Overview of system architecture integrated with CEAZ.

or 64 bits per value. The bit-rate R is $\frac{W}{C}$. Bit-rate R can also be regarded as an average bit length of compressed data. We have $\text{size}(\text{compressed data}) = R * N$, where N is the total number of original data. Assume the ratio of the codewords size to the compressed data size is O , if the codewords overhead is set to be less than 10%, $\frac{S \times B}{S \times B + C \times N} \leq 10\%$.

The symbols generated by dual-quant present a centralized and symmetric distribution, as shown in Figure 5. The generated codewords are highly related to the distribution of symbol frequencies [2]. These good characteristics inspire us to evaluate the similarity of two sets of symbol frequencies using STD. Specifically, assume σ_0 is the STD obtained from the previous data chunk, σ_1 is the STD obtained from the current data chunk, and $\chi = |\sigma_0 - \sigma_1|$. We define a set of thresholds τ_χ and propose the following strategy:

- We will not generate new codewords if $\chi \leq \tau_0$ (two frequencies with similar distributions generate almost identical codewords) but keep using the old codewords;
- We will generate new codewords if $\tau_0 < \chi \leq \tau_1$;
- We will use the offline Huffman codewords if $\chi \geq \tau_1$.

We are processing data that is completely different from the previous data if distribution changes drastically. We need to clear the histogram of compression engine and collect new symbol frequencies. We set τ_0 and τ_1 as 5.18 and 9.69, respectively, after comprehensive experiments (will be discussed).

Note that our design is different from other Huffman coding works in terms of adaptivity. For example, Tian et al. [45] proposed a reduction-based scheme for GPUs that iteratively merges the encoded symbols and adaptively determines the number of merge iterations. However, CEAZ only builds a new codebook for the data chunk when the change of its histogram exceeds a threshold in order to target FPGA with limited resources and low clock frequency.

3.3 Parallel I/O Accelerator

Figure 6 shows the overview of our system architecture integrated with CEAZ compression engine. Our system includes two parts: (1) The host partitions the input dataset and feed the chunked data through the PCIe. Raw data is buffered in high-bandwidth memory (HBM) with 460 GB/s bandwidth and converted into stream data by memory to stream (mm2s) unit. (2) The compression engine compresses the stream data in real-time and output compressed data. Ethernet intellectual property (IP) packs the compressed data according to the network protocol. QSFP28 (fiber optical transceiver) gigabit transceiver (GT) finally outputs packed data into network.

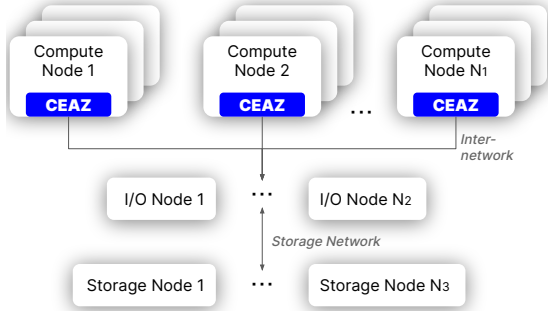


Figure 7. Overview of CEAZ-supported parallel I/O system.

Many scientific applications, such as cosmology simulations, need to periodically dump a huge amount of raw simulation data to the storage for post-hoc analysis and visualization after simulations. Data across all computing nodes needs to be aggregated to the storage node(s). Even though state-of-the-art supercomputers are using InfiniBand interconnect (e.g., 200 Gb/s), it can take hours to complete the data aggregation and save (e.g., 1.5 TB/s of aggregated I/O bandwidth and 4.85 PB memory capacity in Fugaku supercomputer [32]). Therefore, we propose to apply CEAZ to the future HPC systems, as shown in Figure 7.

Specifically, CEAZ is directly integrated into the FPGA-based SmartNIC in each computing node and used to compress the raw data before transmitting it to the storage system via interconnection network. There are two main scenarios to use the CEAZ-compressed data in the storage: (1) checkpoint/restart and (2) post analysis and visualization. Thus, there is no need to change the storage system to adapt to our design, since the data is compressed/decompressed before/after sending/receiving to/from the network adapter. Note that similar to the FPGA-based SmartNIC, the emerging Data Processing Unit (DPUs) [10]—a class of programmable processor—based SmartNIC can also offload and improve application performance for communications and storage. We will extend CEAZ to DPU-based systems in future work.

4 Experimental Evaluation

4.1 Experimental Setup

4.1.1 Experimental Platform. We use two platforms as our testbed. The first platform is Xilinx Alveo U280 Data Center accelerator card, which is equipped with a PCIe Gen4x8 with CCIX to leverage the latest server interconnect infrastructure for high-bandwidth host processors, 8GB HBM2 and 32GB on-board DDR4 DRAM. CEAZ is implemented with Xilinx Vitis unified software platform (v.2020.1) [47]. The second platform (for parallel I/Os) is Summit [38], which is one of the most powerful supercomputers in the world.

4.1.2 Test Datasets. To conduct our evaluation and comparison under realistic scenarios, we use six real-world datasets from the Scientific Data Reduction Benchmarks [36]: ① 1D HACC cosmology particle simulation [17]. ② 1D NWChem

Table 1. Test datasets from Scientific Data Reduction Benchmarks.

	# fields	type	dimensions	size
HACC	6	float	280,953,867	6.3 GB
NWChem	3	double	539,016,059	12.1 GB
Brown	3	double	33,554,433	768.0 MB
CESM	77	float	1,800×3,600	1.9 GB
S3D	11	double	500×500×500	10.2 GB
NYX	6	float	512×512×512	3.0 GB

two-electron repulsion integrals computed over Gaussian-type orbital basis sets [33], ③ 1D Brown Samples synthetic and generated to specified regularity [3], ④ 2D CESM-ATM climate simulation [6], ⑤ 3D S3D Combustion simulation [24], ⑥ 3D NYX AMR-based cosmology simulation [17]. More details can be found in Table 1.

4.2 Resource Utilization and Clock Frequency

Table 2 shows the breakdown of hardware resource utilization of CEAZ. We implement 16 pipelines for single-precision datasets and 8 pipelines for double-precision datasets. Note that our LUT consumption is very close to BurstZ’s (only 1.6% higher). The running frequency based on our measurement is slightly lower than the clock frequency we set (i.e., 265 MHz) but is still around 260 MHz. Note that N/A means the utilization data is not provided in the BurstZ work [39].

Table 2. Hardware resource utilization.

	board	BRAM_18K	DSP	FF	LUT	percent
BurstZ	VCU118	N/A	N/A	N/A	25600	<5%
CEAZ	U250	165	0	17285	26008	<1%

4.3 Evaluation on Offline Codewords and Codewords Update Frequency

We use predefined (offline) codewords at the beginning of the compression process. To prove the effectiveness of our predefined codewords, we evaluate four datasets (i.e., NWChem, HACC, CESM, and S3D) using these codewords with the same value-ranged-based relative error bound of $1e-4$ and compare their compression ratios with the optimal ones, as shown in Figure 8. The orange bars represent the ideal compression ratio achieved by first building Huffman tree and then generating accurate codewords. The blue bars represent the compression ratio by directly using our offline codewords. The compression ratio drops on NWChem, CESM, S3D are 23.3% ~ 51.7%. The compression ratio degradation on HACC is more obvious (i.e., ~ 51.7%); this is because the Lorenzo predictor has low efficiency on HACC dataset, and the distribution of quant code generated by the Lorenzo predictor is not statistically representative. We note that even though HACC’s compression ratio drops more than 51.7%, the compression ratio over $4\times$ can still relieve the communication pressure to a certain extent thanks to our high throughput (will be discussed in Section 4.7).

As aforementioned, frequently updating codewords will decrease the compression ratio due to the overhead of saving

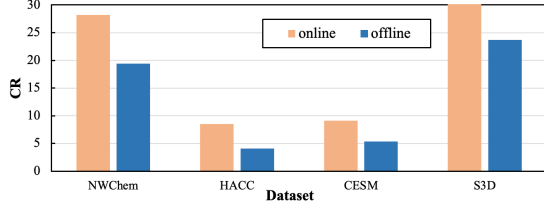


Figure 8. Comparison of compression ratio (CR) between offline codewords and online codewords.

codewords. We evaluate the impact of update frequency on the final compression ratio. We perform the experiments on both CEM and HACC. We set the error bound to the value-range-based relative error bound of $1e-4$. We choose to update the codewords every 1 MB, 2 MB, 4 MB, 16 MB, 32 MB, 64 MB, 128 MB, 256 MB, and 512 MB. We find that the compression ratio is significantly reduced when the update size is smaller than 32, because the overhead of storing the codewords is relatively large. Moreover, we also observe that the compression ratio decreases when the update size is larger than 256 MB. The reason is that the codewords are outdated to reflect the current symbols frequencies. Therefore, we choose 32 MB as our default update size.

4.4 Evaluation on Change of Standard Deviation of Symbol Frequencies

As aforementioned, we use the change of standard deviation of symbol frequencies (i.e., $\chi = |\sigma_0 - \sigma_1|$) to determine when to generate new codewords, use old codewords, or use offline codewords. Using previous codewords under a large χ (a large difference between current and previous distribution) results in a notable drop of compression ratio, while generating new codewords under a small χ (a small difference between current and previous distribution) leads to a high overhead of Huffman coding. Thus, we use experiments to find the suitable thresholds τ_0 and τ_1 . As shown in Figure 9, the drop of compression ratio is less than 5% when $\chi \leq 9.69$, while the drop is over 25% when $\chi \geq 5.18$. So, we set τ_0 and τ_1 to 5.18 and 9.69, respectively, to meet both requirements on compression ratio and performance.

4.5 Evaluation on Fixed-Ratio Mode

As discussed in Section 3, our novel compression engine has two working modes: fixed-accuracy mode (i.e. error-bounded mode) and fixed-ratio mode (i.e., fixed bit-rate mode). The fixed-ratio mode can allow the system have a consistent

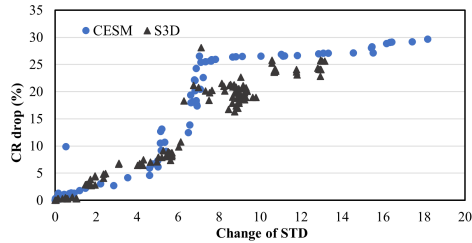


Figure 9. Compression ratio drops with different changes of STD.

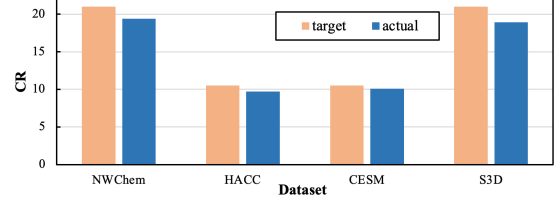


Figure 10. Comparison of target & actual ratio in fixed-ratio mode.

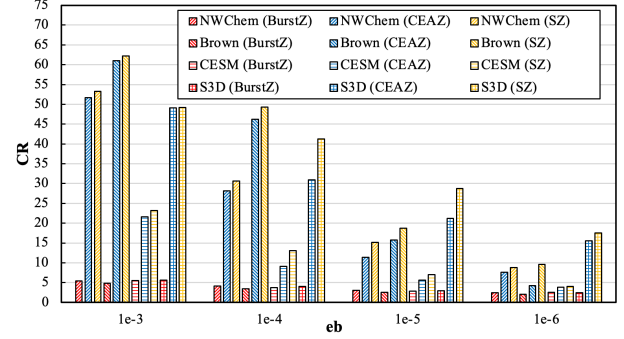


Figure 11. Ratio comparison among BurstZ, CEAZ, SZ.

throughput for data transfer. To verify the effectiveness of our fixed-ratio mode, we set the target compression ratios of 10.5 and 21 for single and double floating-point data, respectively. Figure 10 shows the compression between the target ratio and the actual ratio. The difference is within 15%, which is acceptable in our use case.

4.6 Evaluation on Ratio and Distortion

Compression ratio is defined as the ratio of original data size to the compressed data size. PSNR is a widely used indicator to assess the distortion of data after lossy compression, which is calculated as $PSNR = 20 \cdot \log_{10} \left[\frac{d_{\max} - d_{\min}}{d_i - d_i^*} \right]$. N is the number of data points and d_{\max} and d_{\min} are the maximal and minimal values, respectively. RMSE is the *root mean squared error*, i.e., $\sqrt{\frac{1}{N} \sum_{i=1}^N (d_i - d_i^*)^2}$, where d_i and d_i^* are the original and decompressed data values, respectively. The larger the PSNR, the lower the distortion of reconstructed data, hence more accurate post analysis.

Figure 11 shows the comparison of compression ratio among BurstZ, CEAZ, and CPU-SZ on our test datasets with different value-ranged-based relative error bounds of $1e-3 \sim 1e-6$. The compression ratio of our CEAZ is notably higher than that of BurstZ. CEAZ consistently provides $3 \times \sim 10 \times$ higher compression ratio than BurstZ under the same error bound. Particularly, our CEAZ improves the compression ratio by up to $12 \times$ on the Brown dataset over BurstZ when the error bound is equal to $1e-3$. Compared to the CPU-SZ, the degradation of compression ratio is within 10% on all test datasets and error bounds. This result demonstrates the effectiveness of our adaptive strategy and offline codewords.

We also compare the compression ratio and throughput among LZ4, Gzip, and CEAZ with the best compression mode for LZ4/Gzip. Table 3 illustrates that CEAZ is effective to reduce the scientific data size with high throughput.

Table 3. Comparison of compression ratio and averaged throughput (in GB/s) among LZ4, Gzip, CEAZ, and CPU-SZ on test datasets.

	eb	NWChem	Brown	CESM	S3D	throughput
LZ4	N/A	1.01	1.06	1.18	1.05	1.5
Gzip	N/A	1.05	1.24	1.51	1.14	1.3
CEAZ	1e-4	28.2	46.2	9.1	30.9	16.5
CPU-SZ	1e-4	30.6	49.3	13.1	41.3	0.2

In addition, Table 4 shows the comparison of distortion (PSNR) between CEAZ and CPU-SZ under different error bounds. The degradation of PSNR is within 3 dB under very high PSNRs (all higher than 60 dB).

Table 4. Distortion (i.e., PSNR) comparison between CEAZ and SZ.

eb	NWChem		Brown		CESM		S3D	
	SZ	CEAZ	SZ	CEAZ	SZ	CEAZ	SZ	CEAZ
1e-3	67.5	70.1	64.7	64.8	64.8	63.7	69.2	65.9
1e-4	86.7	90.4	84.7	83.8	85.9	84.3	85.4	87.1
1e-5	105.1	107.7	104.8	104.6	105.3	103.6	104.7	108.6
1e-6	124.9	126.0	124.8	124.5	125.4	124.7	124.9	128.6

4.7 Evaluation on Time, Latency, and Throughput

The time of the entire compression process (excluding the file loading and dumping time) is measured as the period from the moment that FPGA receives the data through the moment that the whole compression is finished with output bytes. We show the comparison of compression time among BurstZ, CEAZ, and CPU-SZ in Table 5. The abbreviation “ebs” represents all error bounds from 1e-3 to 1e-6. We observe that CEAZ reduces the time by up to 67% compared with the second-best BurstZ on the same dataset.

Table 5. Compression time (in second) of different compressors.

	eb	NWChem	Brown	CESM	S3D
BurstZ	1e-3	2.0	3.1e-2	1.8e-1	5.5
BurstZ	1e-4	2.1	3.1e-2	1.8e-1	5.5
BurstZ	1e-5	2.3	4.3e-2	2.7e-1	8.1
BurstZ	1e-6	2.3	4.6e-2	2.7e-1	8.1
CEAZ	ebs	1.0	1.5e-2	8.9e-2	2.7
CPU-SZ	ebs	131.1	2.0	12.0	360.7

Moreover, we evaluate the latency of CPU-SZ, cuSZ, cuZFP, and CEAZ on small datasets, as shown in Table 6. The test small data are chunked from the CESM-ATM dataset. The table illustrates that CEAZ achieves up to 587.8× and 25.6× lower latency than cuSZ and cuZFP, respectively.

Table 6. Latency (μ s) of different lossy compressors on small data.

	CPU-SZ	cuSZ (GPU)	cuZFP (GPU)	CEZA (FPGA)
1 KB	119	423.2	17.9	0.7
4 KB	150	507.6	19.7	1.7
16 KB	466	563.5	27.2	5.5
64 KB	5699	631.7	46.1	20.9

Throughput is defined as the number of data points processed (such as compression) per second. Figure 12 shows the comparison of throughput among BurstZ, CEAZ, and CPU-SZ across four datasets and four error bounds. CEAZ

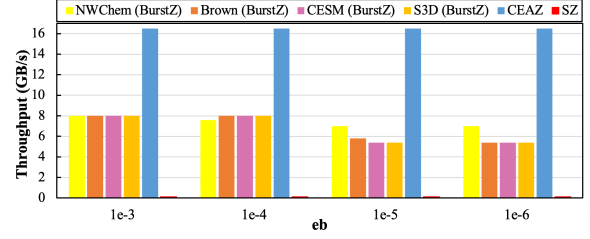


Figure 12. Throughput comparison among BurstZ, CEAZ, CPU-SZ.

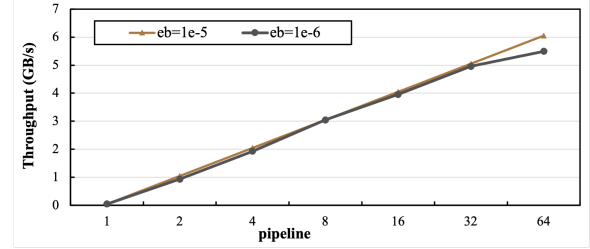


Figure 13. Compression throughputs with multiple pipelines.

can consistently provide about 16 GB/s throughput with different error bound settings, which is 2× higher than BurstZ.

It is worth noting that CEAZ can provide at least 4× higher compression ratio compared to BurstZ. Due to such a high compression ratio (or high data reduction capability), the bandwidth of dumping compressed data (even with the smallest ratio) is still less than the bandwidth capacity of the Ethernet transceiver in our FPGA board (i.e., 100 Gb/s), thereby, the overall throughput has not been bounded by this capacity. Moreover, our clock frequency is around 265 MHz; thus, the throughput could be further improved by increasing the frequency. In addition, compared with the serial CPU-SZ, CEAZ improves the overall throughput by up to 135×.

4.8 Parallel Performance Evaluation

We demonstrate the parallel performance in two ways. First, we evaluate the throughput of CEAZ with different parallel pipelines in the single FPGA board. Second, we evaluate CEAZ with multiple nodes.

4.8.1 Multi-pipeline Evaluation. We choose the CESM-ATM dataset and set the value-range-based error bound to 1e-5 or 1e-6, which is commonly used in the CESM application [34]. We increase the compression pipelines from 1 to 64. Figure 13 illustrates that the throughput increases linearly as the number of pipelines increases (except 64 pipelines with the error bound of 1e-6). CEAZ can achieve this high scalability because (1) our compression engine reads data from HMB2 with a very high bandwidth of 460 GB/s, and (2) our compression engine adopts dual-quant to fully remove the data dependency so that we can process different chunks of the dataset in parallel.

4.8.2 Multi-node Evaluation. We evaluate the performance improvements of MPI-IO and MPI collective operations gained from CEAZ, i.e., MPI_File_write and MPI_Gather.

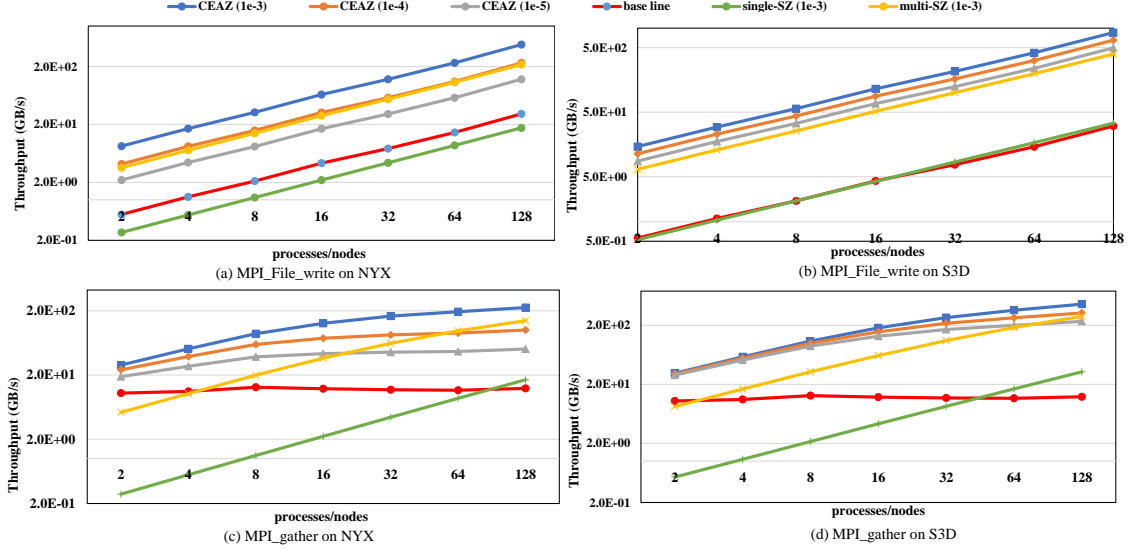


Figure 14. Throughput comparison of CEAZ-accelerated and original MPI_File_write and MPI_Gather on NYX and S3D with different numbers of processes/nodes. “single-SZ” denotes SZ with a single CPU core/node. “multi-SZ” denotes SZ with 32 CPU cores/node.

We conduct our experiments with up to 128 nodes (one process per node). Each node holds a copy of datasets for compression and transmission, i.e., 3.0 GB of NYX and 10.2 GB of S3D per node. Thus, the overall data size for parallel I/O is up to 1.3 TB with 128 nodes. We evaluate CPU-SZ on both a single core and 32 cores with the error bound of 1e-3. Table 7 shows the compression ratio of CPU-SZ and CEAZ on NYX and S3D with different error bounds.

Table 7. Compression ratio of CPU-SZ and CEAZ on NYX and S3D.

	NYX		S3D	
	CPU-SZ	CEAZ	CPU-SZ	CEAZ
1e-3	23.1	20.3	49.2	47.3
1e-4	10.4	8.5	41.3	30.9
1e-5	5.5	4.2	28.8	21.1

Figure 14 (a) and Figure 14 (b) show the MPI-IO throughputs on the NYX and S3D datasets with different approaches. The throughput of original MPI_File_write (without compression) increases as the number of nodes increases and can reach up to 30.51 GB/s with 128 nodes in Summit, as shown as the baselines in the figures. The single-core-SZ-supported MPI_File_write only achieves an overall throughput of 33.75 GB/s (including compression time and time to write compressed data) on S3D when using 128 nodes, which is just 10.6% higher than the baseline. This is because the compression throughput of single-core CPU-SZ (i.e., about 280 MB/s) is not fast enough compared to the state-of-the-art interconnect such as InfiniBand HDR with a bandwidth of 200Gb/s. Note that unlike on S3D, the single-core-SZ-supported MPI_File_write on NYX is slower than the baseline, since the compression ratio of SZ on NYX (i.e., 19.1) is much lower than S3D (i.e., 47.4). The multi-core-SZ-supported MPI_File_write can provide an overall throughput of up to 398.6 GB/s when using 128 nodes, which is 13.1× higher than the baseline. In comparison, CEAZ-supported

MPI_File_write can improve the overall throughput (including compression time and time to write compressed data) by 15.7× and 28.1× on NYX and S3D, respectively.

Figure 14 (c) and Figure 14 (d) show the MPI_Gather throughputs on the NYX and S3D datasets with different approaches. The throughput of original MPI_Gather reaches 12.37 GB/s with 128 nodes in Summit, as shown as the base-lines in the figures. Similar to MPI_File_write, the single-core-SZ-supported MPI_Gather only achieves an overall throughput of up to 32.63 GB/s with 128 nodes, which is just 2.6× higher than the baseline; the multi-core-SZ-supported MPI_Gather can provide an overall throughput of up to 283.9 GB/s when using 128 nodes, which is 22.95× higher than the baseline. In comparison, CEAZ-supported MPI_Gather can improve the overall throughput by 18.1× and 36.9× on NYX and S3D, respectively, due to the high efficiency of CEAZ.

5 Conclusion and Future Work

In this work, we propose CEAZ: a hardware-algorithm co-design of efficient and adaptive lossy compressor for scientific data. To achieve both high compression ratio and throughput, we propose an efficient Huffman coding approach that can adaptively update Huffman codewords online based on our offline generated representative Huffman codewords. We also derive a theoretical analysis to accurately control compression ratio under the error-bounded compression mode, enabling an accurate generation of offline Huffman codewords and a fixed-ratio compression mode. Our evaluation demonstrates that CEAZ outperforms the second-best FPGA-based error-bounded lossy compressor by 2× of throughput and 9.6× of compression ratio. CEAZ improves MPI_File_write and MPI_Gather by up to 28.1× and 36.9×, respectively, with 128 nodes in Summit. We will extend our CEAZ to DPU-based systems in future work.

References

- [1] Ann S Almgren, John B Bell, Mike J Lijewski, Zarija Lukić, and Ethan Van Andel. 2013. Nyx: A massively parallel amr code for computational cosmology. *The Astrophysical Journal* 765, 1 (2013), 39.
- [2] Ian Blanes, Miguel Hernández-Cabronero, Joan Serra-Sagristà, and Michael W Marcellin. 2019. Lower bounds on the redundancy of Huffman codes with known and unknown probabilities. *IEEE Access* 7 (2019), 115857–115870.
- [3] Brown-Samples by Brown University. 2019. <https://sdrbench.github.io/>. Online.
- [4] Martin Burtcher and Paruj Ratanaworabhan. 2008. FPC: A high-speed compressor for double-precision floating-point data. *IEEE Trans. Comput.* 58, 1 (2008), 18–31.
- [5] Franck Cappello, Sheng Di, Sihuan Li, Xin Liang, Ali Murat Gok, Dingwen Tao, Chun Hong Yoon, Xin-Chuan Wu, Yuri Alexeev, and Fred-eric T Chong. 2019. Use cases of lossy compression for floating-point data in scientific data sets. *The International Journal of High Performance Computing Applications* (2019).
- [6] Community Earth System Model (CESM) Atmosphere Model. 2019. <http://www.cesm.ucar.edu/models/>. Online.
- [7] cuZFP. 2021. https://github.com/LLNL/zfp/tree/develop/src/cuda_zfp.
- [8] Sheng Di and Franck Cappello. 2016. Fast error-bounded lossy HPC data compression with SZ. In *2016 IEEE International Parallel and Distributed Processing Symposium*. IEEE, 730–739.
- [9] Sheng Di and Franck Cappello. 2016. Fast error-bounded lossy HPC data compression with SZ. In *2016 IEEE International Parallel and Distributed Processing Symposium*. IEEE, IEEE, Chicago, IL, USA, 730–739.
- [10] DPU. 2021. <https://blogs.nvidia.com/blog/2020/05/20/whats-a-dpu-data-processing-unit/>. Online.
- [11] Daniel Firestone, Andrew Putnam, Sambhrama Mundkur, Derek Chiou, Alireza Dabagh, Mike Andrewartha, Hari Angepat, Vivek Bhanu, Adrian Caulfield, Eric Chung, et al. 2018. Azure accelerated networking: Smartnics in the public cloud. In *15th {USENIX} Symposium on Networked Systems Design and Implementation ({NSDI} 18)*. 51–66.
- [12] Mike Folk, Gerd Heber, Quincey Koziol, Elena Pourmal, and Dana Robinson. 2011. An overview of the HDF5 technology suite and its applications. In *Proceedings of the EDBT/ICDT 2011 Workshop on Array Databases*. 36–47.
- [13] Tong Geng, Tianqi Wang, Chunshu Wu, Chen Yang, Wei Wu, Ang Li, and Martin C. Herbordt. 2019. O3BNN: an out-of-order architecture for high-performance binarized neural network inference with fine-grained pruning. In *Proceedings of the ACM International Conference on Supercomputing*. ACM, Denver, CO, USA, 461–472.
- [14] Ali Murat Gok, Sheng Di, Yuri Alexeev, Dingwen Tao, Vladimir Mironov, Xin Liang, and Franck Cappello. 2018. Pastr: Error-bounded lossy compression for two-electron integrals in quantum chemistry. In *2018 IEEE international conference on cluster computing (CLUSTER)*. IEEE, 1–11.
- [15] William Gropp, Ewing Lusk, Nathan Doss, and Anthony Skjellum. 1996. A high-performance, portable implementation of the MPI message passing interface standard. *Parallel computing* 22, 6 (1996), 789–828.
- [16] Pascal Grosset, Christopher Biwer, Jesus Pulido, Arvind Mohan, Ayan Biswas, John Patchett, Terece Turton, David Rogers, Daniel Livescu, and James Ahrens. 2020. Foresight: analysis that matters for data reduction. In *2020 SC20: International Conference for High Performance Computing, Networking, Storage and Analysis (SC)*. IEEE Computer Society, 1171–1185.
- [17] HACC team (ECP EXASKY). 2019. <https://sdrbench.github.io/>. Online.
- [18] Pouya Haghi, Anqi Guo, Qingqing Xiong, Rushi Patel, Chen Yang, Tong Geng, Justin T Broadus, Ryan Marshall, Anthony Skjellum, and Martin C Herbordt. 2020. FPGAs in the Network and Novel Communicator Support Accelerate MPI Collectives. In *2020 IEEE High Performance Extreme Computing Conference (HPEC)*. IEEE, 1–10.
- [19] D. A. Huffman. 1952. A Method for the Construction of Minimum-Redundancy Codes. *Proceedings of the IRE* 40, 9 (Sep. 1952), 1098–1101.
- [20] Lawrence Ibarria, Peter Lindstrom, Jarek Rossignac, and Andrzej Szymczak. 2003. Out-of-core compression and decompression of large n-dimensional scalar fields. In *Computer Graphics Forum*, Vol. 22. Wiley Online Library, 343–348.
- [21] Sian Jin, Pascal Grosset, Christopher M Biwer, Jesus Pulido, Jiannan Tian, Dingwen Tao, and James Ahrens. 2020. Understanding GPU-Based Lossy Compression for Extreme-Scale Cosmological Simulations. *arXiv preprint arXiv:2004.00224* (2020).
- [22] Sian Jin, Jesus Pulido, Pascal Grosset, Jiannan Tian, Dingwen Tao, and James Ahrens. 2021. Adaptive Configuration of In Situ Lossy Compression for Cosmology Simulations via Fine-Grained Rate-Quality Modeling. *arXiv preprint arXiv:2104.00178* (2021).
- [23] Ryan Kastner, Janarbek Matai, and Stephen Neuendorffer. 2018. Parallel programming for FPGAs. *arXiv preprint arXiv:1805.03648* (2018).
- [24] Hemanth Kolla. 2019. <https://sdrbench.github.io/>. Online.
- [25] Sohan Lal, Jan Lucas, and Ben Juurlink. 2017. E² 2MC: Entropy Encoding Based Memory Compression for GPUs. In *2017 IEEE International Parallel and Distributed Processing Symposium (IPDPS)*. IEEE, 1119–1128.
- [26] Xin Liang, Sheng Di, Dingwen Tao, Sihuan Li, Shaomeng Li, Hanqi Guo, Zizhong Chen, and Franck Cappello. 2018. Error-Controlled Lossy Compression Optimized for High Compression Ratios of Scientific Datasets. (2018).
- [27] Peter Lindstrom. 2014. Fixed-rate compressed floating-point arrays. *IEEE Transactions on Visualization and Computer Graphics* 20, 12 (2014), 2674–2683.
- [28] Peter Lindstrom and Martin Isenburg. 2006. Fast and efficient compression of floating-point data. *IEEE Transactions on Visualization and Computer Graphics* 12, 5 (2006), 1245–1250.
- [29] Jay F Lofstead, Scott Klasky, Karsten Schwan, Norbert Podhorszki, and Chen Jin. 2008. Flexible IO and integration for scientific codes through the adaptable IO system (ADIOS). In *Proceedings of the 6th international workshop on Challenges of large applications in distributed environments*. 15–24.
- [30] Tao Lu, Qing Liu, Xubin He, Huizhang Luo, Eric Suchyta, Jong Choi, Norbert Podhorszki, Scott Klasky, Mathew Wolf, Tong Liu, et al. 2018. Understanding and modeling lossy compression schemes on HPC scientific data. In *2018 IEEE International Parallel and Distributed Processing Symposium*. IEEE, 348–357.
- [31] Huizhang Luo, Dan Huang, Qing Liu, Zhenbo Qiao, Hong Jiang, Jing Bi, Haitao Yuan, Mengchu Zhou, Jinzhen Wang, and Zhenlu Qin. 2019. Identifying Latent Reduced Models to Precondition Lossy Compression. In *2019 IEEE International Parallel and Distributed Processing Symposium*. IEEE.
- [32] Masahiro Nakao, Koji Ueno, Katsuki Fujisawa, Yuetsu Kodama, and Mitsuhisa Sato. 2020. Performance Evaluation of Supercomputer Fugaku using Breadth-First Search Benchmark in Graph500. In *2020 IEEE International Conference on Cluster Computing (CLUSTER)*. IEEE, 408–409.
- [33] NWChem - Open Source High-Performance Computational Chemistry. 2019. <https://nwchemgit.github.io/>. Online.
- [34] Andrew Poppick, Joseph Nardi, Noah Feldman, Allison H Baker, Alexander Pinard, and Dorit M Hammerling. 2020. A statistical analysis of lossily compressed climate model data. *Computers & Geosciences* 145 (2020), 104599.
- [35] Andrew Putnam, Adrian M Caulfield, Eric S Chung, Derek Chiou, Kypros Constantinides, John Demme, Hadi Esmaeilzadeh, Jeremy Fowers, Gopi Prashanth Gopal, Jan Gray, et al. 2014. A reconfigurable fabric for accelerating large-scale datacenter services. In *2014 ACM/IEEE 41st International Symposium on Computer Architecture (ISCA)*. IEEE, 13–24.

- [36] Scientific Data Reduction Benchmarks. 2019. <https://sdrbench.github.io/>. Online.
- [37] Seung Woo Son, Zhengzhang Chen, William Hendrix, Ankit Agrawal, Wei-keng Liao, and Alok Choudhary. 2014. Data compression for the exascale computing era-survey. *Supercomputing Frontiers and Innovations* 1, 2 (2014), 76–88.
- [38] Summit. 2021. <https://www.olcf.ornl.gov/olcf-resources/compute-systems/summit/>. Online.
- [39] Gongjin Sun, Seongyoung Kang, and Sang-Woo Jun. 2020. BurstZ: a bandwidth-efficient scientific computing accelerator platform for large-scale data. In *Proceedings of the 34th ACM International Conference on Supercomputing*. 1–12.
- [40] Dingwen Tao, Sheng Di, Zizhong Chen, and Franck Cappello. 2017. In-depth exploration of single-snapshot lossy compression techniques for N-body simulations. In *2017 IEEE International Conference on Big Data*. IEEE, 486–493.
- [41] Dingwen Tao, Sheng Di, Zizhong Chen, and Franck Cappello. 2017. Significantly improving lossy compression for scientific data sets based on multidimensional prediction and error-controlled quantization. In *2017 IEEE International Parallel and Distributed Processing Symposium*. IEEE, 1129–1139.
- [42] Dingwen Tao, Sheng Di, Xin Liang, Zizhong Chen, and Franck Cappello. 2019. Optimizing Lossy Compression Rate-Distortion from Automatic Online Selection between SZ and ZFP. *IEEE Transactions on Parallel and Distributed Systems* (2019).
- [43] Jiannan Tian, Sheng Di, Chengming Zhang, Xin Liang, Sian Jin, Dazhao Cheng, Dingwen Tao, and Franck Cappello. 2020. Wavesz: A hardware-algorithm co-design of efficient lossy compression for scientific data. In *Proceedings of the 25th ACM SIGPLAN Symposium on Principles and Practice of Parallel Programming*. 74–88.
- [44] Jiannan Tian, Sheng Di, Kai Zhao, Cody Rivera, Megan Hickman Fulp, Robert Underwood, Sian Jin, Xin Liang, Jon Calhoun, Dingwen Tao, and Franck Cappello. 2020. cuSZ: An Efficient GPU-Based Error-Bounded Lossy Compression Framework for Scientific Data. (2020), 3–15.
- [45] Jiannan Tian, Cody Rivera, Sheng Di, Jieyang Chen, Xin Liang, Dingwen Tao, and Franck Cappello. 2021. Revisiting Huffman Coding: Toward Extreme Performance on Modern GPU Architectures. In *2021 IEEE International Parallel and Distributed Processing Symposium (IPDPS), Portland, OR, USA, May 17-21, 2021*. IEEE, 881–891.
- [46] Vitis Libraries. 2020. https://github.com/Xilinx/Vitis_Libraries/. Online.
- [47] Vitis Unified Software Platform. 2020. <https://www.xilinx.com/products/design-tools/vitis/vitis-platform.html>. Online.
- [48] Lipeng Wan, Matthew Wolf, Feiyi Wang, Jong Youl Choi, George Ostrouchov, and Scott Klasky. 2017. Analysis and modeling of the end-to-end i/o performance on olcf’s titan supercomputer. In *2017 IEEE 19th International Conference on High Performance Computing and Communications; IEEE 15th International Conference on Smart City; IEEE 3rd International Conference on Data Science and Systems (HPCC/SmartCity/DSS)*. IEEE, 1–9.
- [49] Lipeng Wan, Matthew Wolf, Feiyi Wang, Jong Youl Choi, George Ostrouchov, and Scott Klasky. 2017. Comprehensive measurement and analysis of the user-perceived I/O performance in a production leadership-class storage system. In *2017 IEEE 37th International Conference on Distributed Computing Systems (ICDCS)*. IEEE, 1022–1031.
- [50] Xin-Chuan Wu, Sheng Di, Emma Maitreyee Dasgupta, Franck Cappello, Hal Finkel, Yuri Alexeev, and Frederic T Chong. 2019. Full-state quantum circuit simulation by using data compression. In *Proceedings of the International Conference for High Performance Computing, Networking, Storage and Analysis*. 1–24.
- [51] Qingqing Xiong, Rushi Patel, Chen Yang, Tong Geng, Anthony Skjelum, and Martin C Herbordt. 2019. Ghostsz: A transparent fpga-accelerated lossy compression framework. In *2019 IEEE 27th Annual International Symposium on Field-Programmable Custom Computing Machines (FCCM)*. IEEE, 258–266.
- [52] ZHW - ZFP Hardware Implementation. 2021. <https://github.com/LLNL/zhw/>. Online.